

# New insights on seismic activity in the southeastern Korean Peninsula from the Gyeongju Hi-density Broadband Seismic Network (GHBSN)

Dabeen Heo<sup>1</sup>, Tae-Seob Kang<sup>1\*</sup>, Minook Kim<sup>1,2</sup>, Byeong Seok Ahn<sup>1</sup>, Hobin Lim<sup>3</sup>, Jaeseoung Han<sup>4</sup>, Kwang-Hee Kim<sup>5</sup>, Junkee Rhie<sup>4</sup>, YoungHee Kim<sup>4</sup>, and Jin-Han Ree<sup>6</sup>

<sup>1</sup>Division of Earth Environmental System Science, Pukyong National University, Busan 48513, Republic of Korea

<sup>2</sup>Department of Structure and Site Evaluation, Korea Institute of Nuclear Safety, Daejeon 34142, Republic of Korea

<sup>3</sup>Earthquake Research Center, Korea Institute of Geoscience and Mineral Resources, Daejeon 34132, Republic of Korea

<sup>4</sup>School of Earth and Environmental Sciences, Seoul National University, Seoul 08826, Republic of Korea

<sup>5</sup>Department of Geological Sciences, Pusan National University, Busan 46241, Republic of Korea

<sup>6</sup>Department of Earth and Environmental Sciences, Korea University, Seoul 02841, Republic of Korea

**ABSTRACT:** The 2016 magnitude ( $M_W$ ) 5.5 Gyeongju earthquake, which occurred in Korea near assumed epicenters of several substantial historical earthquakes and Quaternary fault segments, underscores the importance of seismic hazard assessment in the region. However, uncertainties about potential seismic sources make evaluating the potential for a moderate-to-large earthquake challenging. Microearthquake monitoring through a dense seismic network can provide crucial insights into the regional seismic characteristics. An extensive temporary seismic array known as the Gyeongju Hi-density Broadband Seismic Network (GHBSN) was established to investigate microearthquake activity in the southeastern Korean Peninsula. This included the zone of aftershocks from the 2016 Gyeongju earthquake sequence. The GHBSN comprises 200 broadband stations located at approximately 4.5 km intervals in an area of approximately  $60 \times 60 \text{ km}^2$  around the epicenter of the mainshock. A total of 4,773 events were detected from November 2017 to December 2021, including 3,935 events within the GHBSN. The detected events were categorized into five seismic regions excluding quarry blasting sites, that is, the 2016 Gyeongju earthquake region, eastern part of the Ulsan Fault, 2017 Pohang earthquake region, eastern offshore Gyeongju, and western part of the Miryang Fault. A local magnitude scale was developed for the southeastern Korean Peninsula using events detected through the GHBSN. This reflects the distance attenuation and site conditions of the GHBSN stations for earthquakes. An event catalog was created using two automatic detection methods based on the measurement of the energy ratio. This provided high-resolution hypocenter parameters at a completeness magnitude ( $M_C$ ) of 0.0 despite the seismic environment of the network being exposed to high cultural noise. The Gutenberg-Richter b-value was estimated as  $0.82 \pm 0.02$  for all events and  $1.01 \pm 0.02$  for those inside GHBSN. This implies that the seismicity reflects a representative intraplate seismic environment. Testing the obtainability of the focal mechanism solutions showed that the GHBSN outperformed the regional network. Depending on the relationship between the magnitude and frequency of earthquakes, a relatively large number of small earthquakes can provide detailed information on the geometric properties of the causative faults and the state of the acting stress. High-precision microearthquake observation and analysis through GHBSN could provide an unprecedented opportunity with seismic datasets to understand the seismogenesis of the southeastern Korean Peninsula, including the zone of aftershocks of the 2016 Gyeongju earthquake.

**Key words:** Gyeongju Hi-density Broadband Seismic Network, The 2016 Gyeongju earthquake sequence, microearthquake activity, causative faults, seismogenesis

Manuscript received March 13, 2023; Manuscript accepted January 18, 2024

Editorial responsibility: Tae-Kyung Hong

\*Corresponding author:

Tae-Seob Kang

Division of Earth Environmental System Science, Pukyong National University, 45, Yongso-ro, Nam-Gu, Busan 48513, Republic of Korea  
Telephone: +82-51-629-6632, E-mail: tskang@pknu.ac.kr

**Electronic supplementary material**

The online version of this article (<https://doi.org/10.1007/s12303-024-0003-7>) contains supplementary material, which is available to authorized users.

©The Association of Korean Geoscience Societies and Springer 2024

## 1. INTRODUCTION

The Korean Peninsula is a stable continental region and is located 1,000 km far from the plate boundary (Fig. 1a). Compared to plate boundary regions, intraplate regions have relatively low to moderate seismicity, and earthquakes have varying occurrence frequencies and sporadic distributions (Talwani, 2017). Intraplate earthquakes occur in pre-existing weak zones where stress is

concentrated and fundamentally related to geological structures such as faults. Therefore, understanding the spatiotemporal distribution and source mechanism of microearthquakes is essential for investigating the properties of seismic sources, regional stress fields, and geological structures. Monitoring aftershocks following a large earthquake with a dense seismic array is vital for unraveling detailed seismic source characteristics and fault geometries.

Hundreds of historical earthquakes have been found (Lee and Jin, 1991; Lee and Yang, 2006), and Quaternary faults have been identified on the southeastern Korean Peninsula (Kyung and Chang, 2001; Kyung, 2003; Ree et al., 2003; Park et al., 2006; Cheon et al., 2020), particularly in the vicinity of the Yangsan Fault system. Therefore, the potential for possibility of moderate-to-large earthquakes and the reactivation of faults in the southeastern Korean Peninsula has been raised in various studies. However, despite records of the damage caused by historical earthquakes (Lee and Yang, 2006), it is difficult to constrain the source properties of historical earthquakes. This can lead to a

high level of uncertainty in seismic hazard assessments. With the occurrence of the 2016  $M_w$  5.5 Gyeongju earthquake (Kim et al., 2016a, 2018a; Kim et al., 2016b, 2017; Hong et al., 2017; Son et al., 2018; Woo et al., 2019b) and the 2017  $M_w$  5.5 Pohang earthquake (Grigoli et al., 2018a; Kim et al., 2018b; Lee et al., 2019; Woo et al., 2019a, 2020; Lim et al., 2020), the need for dense seismic network observation has emerged.

The 2016  $M_w$  5.5 Gyeongju earthquake, that is, the mainshock of the Gyeongju earthquake sequence, occurred on the southeastern part of the Korean Peninsula at 11:32:54 (Universal Time) on September 12, 2016 (Fig. 1c). This earthquake was preceded by several foreshocks, including  $M_w$  5.1, which occurred 50 min before the mainshock. After the mainshock, aftershocks continued, including the  $M_w$  4.4 event on September 19, 2016, which was the largest aftershock of the sequence. The rupture characteristics of the mainshock and their association with surface fault traces have been investigated (Hong et al., 2017; Kim et al., 2017; Kim et al., 2018a; Son et al., 2018; Uchide and Song, 2018; Woo et al., 2019b). The subsurface fault was named the Naenam Fault (Lim

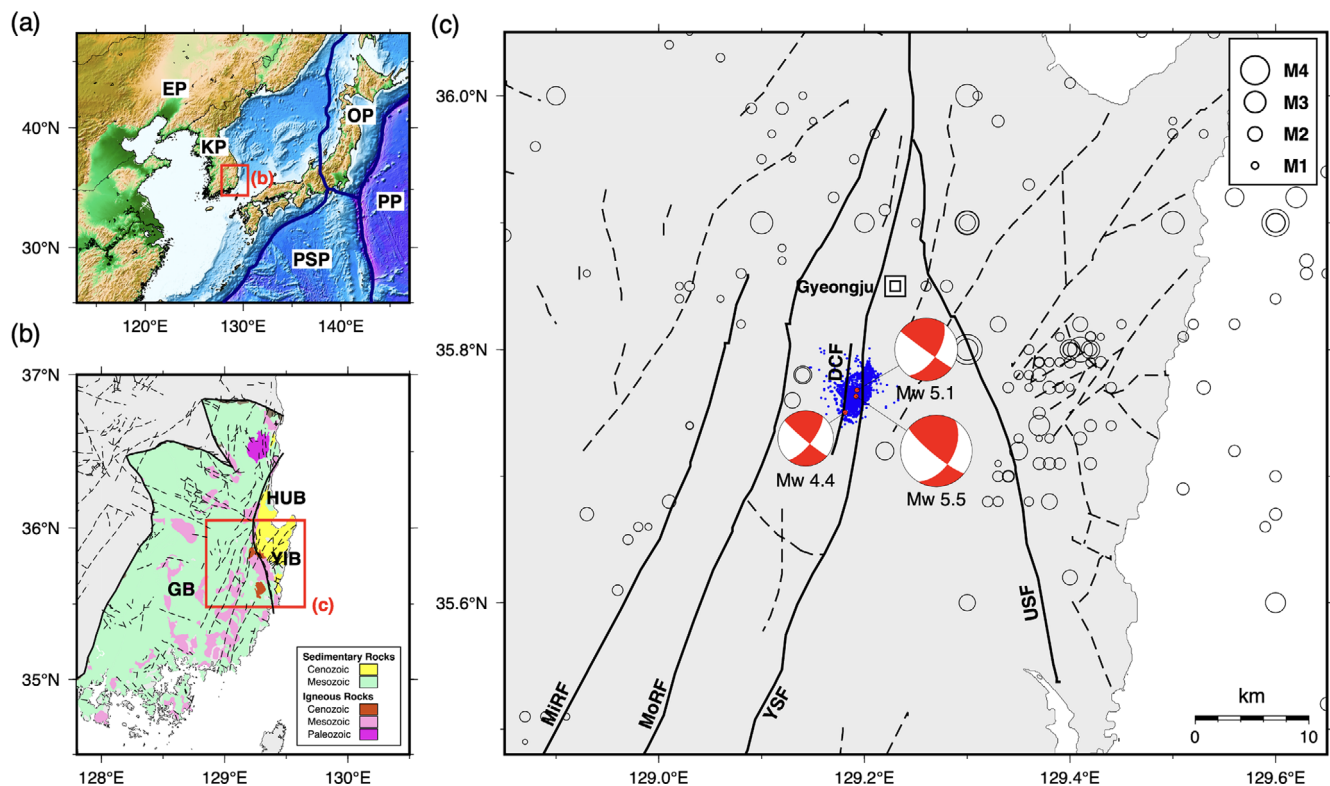


**Fig. 1.** Map of the 2016  $M_w$  5.5 Gyeongju earthquake. (a) Location and tectonic framework of the Korean Peninsula and its surrounding region. (b) Geological setting of the southeastern part of the Korean Peninsula (Chwae et al., 1995; Kang and Shin, 2006). (c) Epicenters of the 2016 Gyeongju earthquake sequence with background seismicity, marked by open gray circles scaled by magnitudes, from January 1, 1978, to September 11, 2016, that occurred before the 2016  $M_w$  5.5 Gyeongju earthquake (KMA). Blue dots denote the aftershocks of the 2016 Gyeongju earthquake (Woo et al., 2019b). Red beach balls show the focal mechanisms of the  $M_w$  5.1 foreshock,  $M_w$  5.5 mainshock, and the  $M_w$  4.4 aftershock determined using the P-wave first motion polarity method. The solid line indicates geological faults with inferred faults marked by dash lines. Lineaments of the study area were digitized from the tectonic map of Korea at a scale of 1:1,000,000 (Hwang et al., 2001). The urban area of Gyeongju City is marked by a double square. KP: Korean Peninsula; EP: Eurasian Plate; OP: Okhotsk Plate; PP: Pacific Plate; PSP: Philippine Sea Plate; GB: Gyeongsang Basin; HUB: Hupo bank and basin; YIB: Yeonil Basin; YSF: Yangsan Fault; MoRF: Moryang Fault; MiRF: Miryang Fault; USF: Ulsan Fault; DCF: Deokcheon Fault.

et al., 2021).

A dense seismic network provides unprecedented opportunities for microearthquake detection and high-resolution seismic imaging. Seismic network data can be used to show detailed subsurface 3-D fault structure in the focal area of an earthquake and to establish a long-term monitoring system against seismic hazards. It can be used to evaluate the seismic hazard potential for a region considering existing, but unruptured, fault areas and to estimate the maximum ground motion for critical infrastructures.

We constructed a high-density seismic network in and around Gyeongju, hereafter referred to as the Gyeongju Hi-density Broadband Seismic Network (GHBSN), to obtain high-quality seismic waveform data. Waveform data have been corrected for misalignment based on the polarization of P-waves from regional and teleseismic earthquakes (Seo et al., 2022). Featuring a denser distribution of seismic stations than regional seismic stations, the GHBSN is expected to show previously unidentified seismological and geological features with enhanced resolution. We created an intensive earthquake catalog from automatic earthquake detection methods based on the measurement of the energy ratio using the GHBSN and evaluated the network performance by comparing it with a regional seismic network in South Korea.

## 2. GEOLOGICAL AND TECTONIC SETTINGS

The Korean Peninsula is situated within the Eurasian Plate. However, at its eastern margin, the Japan Trench and Nankai Trough are located to the southeast and south, respectively (Fig. 1a). Although the Korean Peninsula is currently an intraplate area, it constituted a continental magmatic arc with the Japanese Islands from the early Mesozoic to the middle Tertiary. At this time, a back-arc extension separated it from the peninsula (Chough et al., 2000). The focal mechanism solutions for earthquakes indicate that the Korean Peninsula is in a compressional regime with an ENE-WSW or E-W maximum horizontal stress direction (Jun, 1990; Kim et al., 2006a; Chang et al., 2010; Jun and Jeon, 2010). The regional stress field is likely related to the subduction of the Pacific and Philippine plates under the Eurasian plate, as well as partly to the collision between the Indian and Eurasian plates (Molnar and Tapponnier, 1975; Jolivet et al., 1994).

The epicenters of the 2016 Gyeongju earthquake sequence are located in the Cretaceous Gyeongsang Basin. This is a retro-arc area consisting of non-marine siliciclastic and volcanoclastic sedimentary rocks, and volcanic rocks intruded by Cretaceous and Tertiary granitoids (Chough et al., 2000; Chough and Sohn, 2010). There are several small-scale Tertiary basins, including the Pohang Basin, along the southeastern coast of the peninsula,

which developed during Miocene back-arc spreading. Given that the southeastern Korean Peninsula has experienced at least one cycle of tectonic inversion (Chough et al., 2000; Ree et al., 2003), it has complex fault structures. The most prominent regional faults are the NNE-striking Yangsan, Moryang, and Miryang faults and the NNW-striking Ulsan Fault (Ree et al., 2003). Most reported Quaternary faults occur along the Yangsan and Ulsan faults (Park et al., 2006). The Yangsan Fault system has undergone multiple deformations, of which NNE-trending dextral strike-slip faulting is the most predominant, with a length of approximately 170–200 km (Kyung, 2003). Its horizontal displacement was estimated to be 21.3 km via the correlation of granites (Hwang et al., 2004).

## 3. GYEONGJU HI-DENSITY BROADBAND SEISMIC NETWORK

### 3.1. Network Construction and Data Archiving

The GHBSN consists of 200 broadband seismic stations used to identify small-magnitude earthquakes and investigate the subsurface structure in Gyeongju. The GHBSN was deployed in an area of  $60 \times 60 \text{ km}^2$  around the epicenter of the mainshock. The average interval between stations was 4–5 km (Fig. 2). Given the available number of stations (200) and the square-shaped target region of this project around the aftershocks of the 2016 Gyeongju earthquake, the locations of these stations were designed to be uniform. We considered the level of cultural noise to have a lower priority than the uniformity of station distribution. For example, the GHBSN covers the urban area of Gyeongju, with a population of 20,000 (Figs. 1 and 2).

Deployment of the 200 stations began on November 1, 2017, and were completed on September 8, 2019, spreading from the 2016 Gyeongju earthquake (Fig. 2a). We divided the entire deployment period into phases I, II, III, and IV in terms of the rapid increase in the number of stations. Phase I was from November 1, 2017, when seven pilot stations were deployed on January 31, 2019. Phase II began February 1, 2019, when a total of 42 stations were deployed on March 16, 2019. Phase III was from March 17, 2019, when a total of 117 stations were deployed, to September 7, 2019, when 200 GHBSN stations were deployed. Phase IV was from September 8, 2019, to December 31, 2021, during which 200 stations were used for analysis. The progressive deployment spread from the epicenter of the 2016 Gyeongju earthquake throughout the phases I, II, and III is plotted in Figure 2a. The retardation from Phase I to Phase II stems from the modification of the project plan for a large array.

The seismometer was a Trillium Compact Posthole with a cutoff frequency of 120 s, manufactured by Nanometrics Inc.

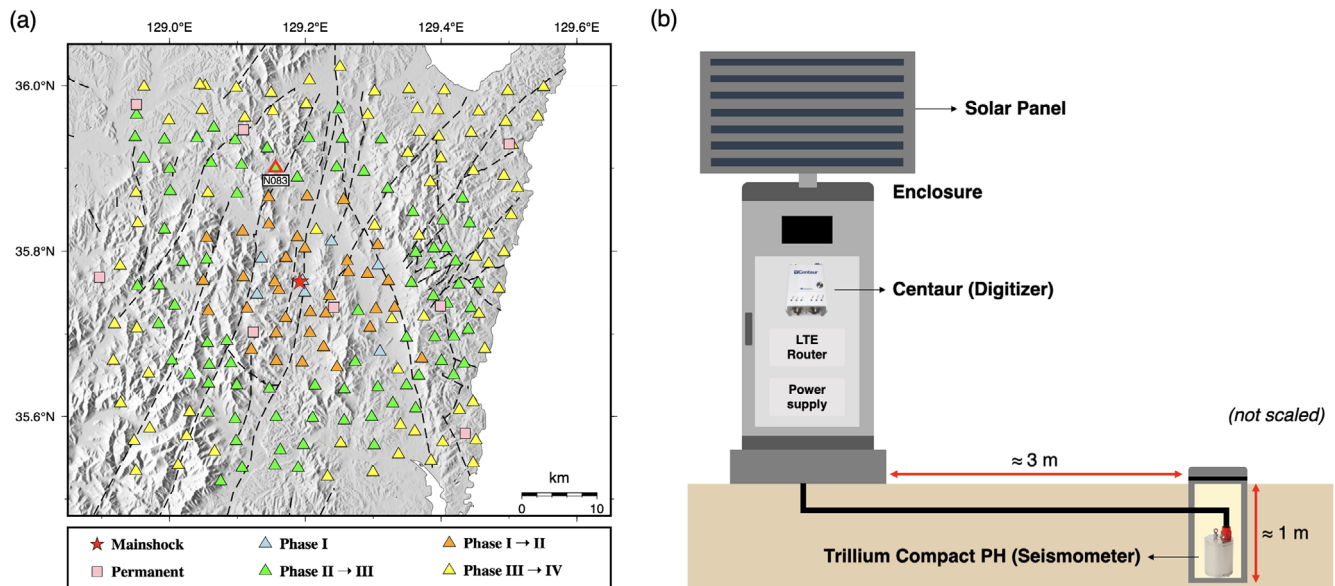


**Fig. 2.** The Gyeongju Hi-density Broadband Seismic Network (GHBSN). (a) Map of the GHBSN. The red star is the epicenter of the 2016 Mw 5.5 Gyeongju earthquake. Pink squares indicate permanent stations operated by KMA and KIGAM. (b) Schematics for the single station of the GHBSN.

(Fig. 2). The seismometer was buried beneath the surface at a depth of 1 m approximately to mitigate cultural noise. The sampling rate was set to 200 Hz. Data were transported remotely for storage at physically distant sites, such as Pukyong National University,

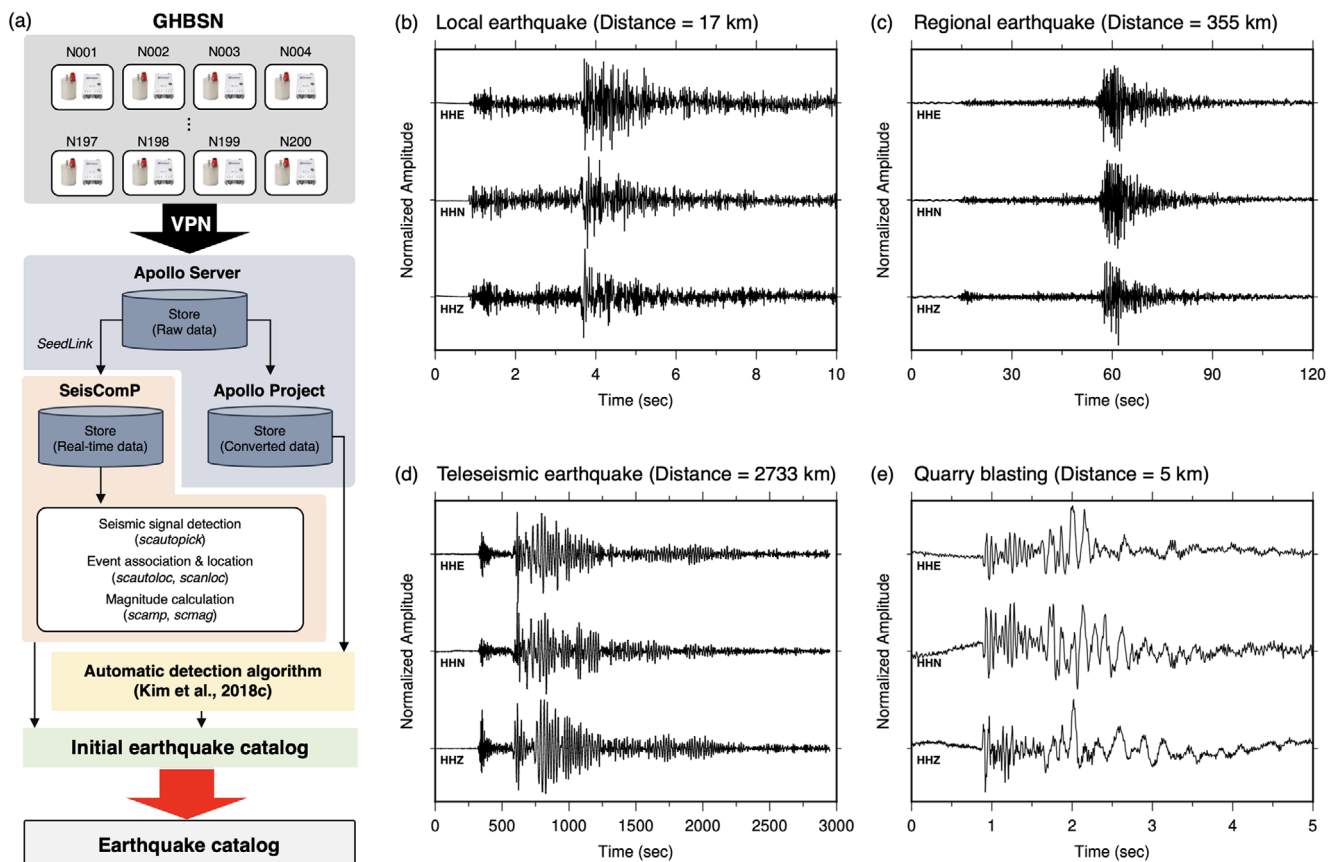


**Fig. 3.** Earthquake monitoring system. (a) Simplified flowchart from remote data acquisition to automate the process of detecting and locating earthquakes. (b–e) Examples of the waveforms at the station N083 of the GHBSN, normalized by the maximum amplitude. HHE, HHN, and HHZ stand for the east, north, and vertical components, respectively.

Seoul National University, and the Korea Institute of Nuclear Safety, via commercial Long-Term Evolution telecommunication (Fig. 3). The final data format was miniSEED (Standard for the Exchange of Earthquake Data; Ahern et al., 2009). Power was supplied using a photovoltaic system. When available, an electric power line was used. We used the commercial programs *Apollo Server* and *Apollo Project* provided by Nanometrics Inc. for data archiving. The *Apollo Server* transfers the seismic data, thereby minimizing the data gap. The *Apollo Project* converts the internal file format to miniSEED. In a separate channel, the data stream branched out from the stage at the *Apollo Server* (Fig. 3a). This stream was transferred and saved via protocols *seedlink* and *slarchive*, respectively, which are compatible with the software package SeisComP (Helmholtz-Centre Potsdam – GFZ German Research Center for Geosciences and GEMPA GmbH, 2008). Figure 3b–e shows examples of seismic waveforms recorded in the GHBSN.

### 3.2. Background Seismic Noise

We observed temporal and spatial variations in the level of background seismic noise in the GHBSN. This analysis was

performed including during the deployment in 2017–2020 to determine the systematic error that could increase the noise. The initial design in which the seismometer was relatively close to the enclosure amplified the noise from the enclosure swaying in the wind (early Phase I; Fig. 4b). We followed a protocol in which the seismometer was placed at least 3 m away from the enclosure and buried approximately 1 m beneath the surface (Fig. 2). This protocol was retrograded to seven deployed stations in Phase I.

Figure 4 shows examples of the probabilistic power spectral density (PPSD) at stations N004, N011, and N025 (McNamara and Buland, 2004). The wind-driven noise at 10–100 s, owing to the short distance between the seismometer and enclosure, was mitigated (Fig. 4a, b). At 100 s, the noise was reduced by approximately 30 dB (Fig. 4a, b).

We found that stations with relatively strong short-period noise in 0.05–1 s are collocated around regions where high cultural noise is expected. For example, N011 in Figure 4c, d has a lower level of noise than N025 in Figure 4e, f in 0.05–1 s. The maps of the noise at 0.05–1 s for the day and night show a spatial correlation between the noisy stations and the developed area.

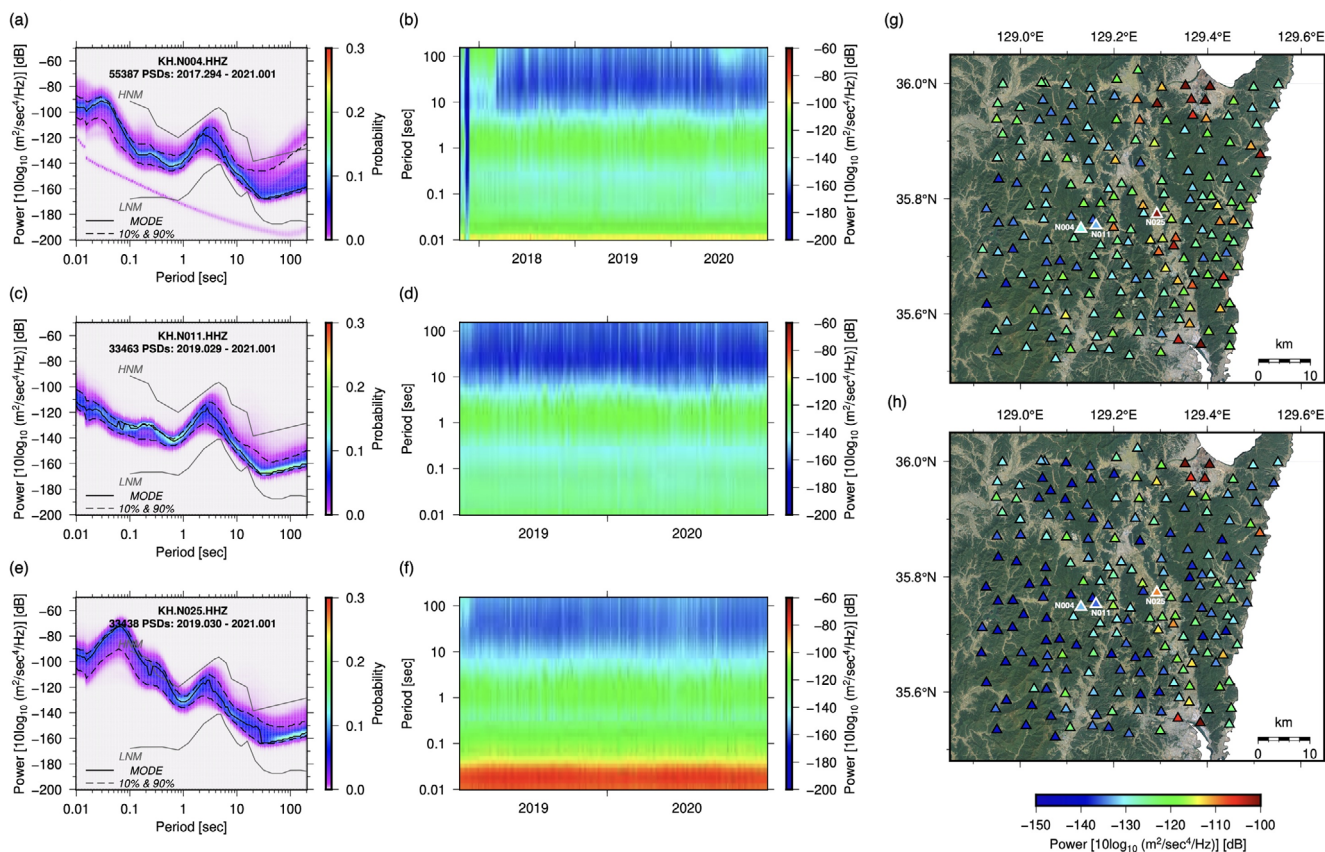


**Fig. 4.** Ambient noise of the GHBSN. (a) Probabilistic power spectral density (PPSD) of vertical components of station N004 from October 21, 2017, to January 1, 2021. (b) Temporal plot of the PPSD in (a). (c) PPSD of N011 from January 29, 2019, to January 1, 2021. (d) Temporal plot of the PPSD in (c). (e) PPSD of N025 from January 30, 2019, to January 1, 2021. (f) Temporal plot of the PPSD in (e). (g) Map of the ambient noise in (g) day and (h) night in 1–20 Hz, overlaid on satellite image from Google Earth. Forest and developed areas are distinguished with dark green and faint-green-to-grey colors, respectively. Locations of the N004, N011, and N025 are marked from west to east in order with thick, white-outlined triangles.

This can be recognized as a gray-to-faint-green zone on the satellite image (Fig. 4g, h). Similarly, the low-noise stations were located in the forest (Fig. 4g, h).

Background noise levels were compared between stations of the KMA network (Korea Meteorological Administration, 2021) in the region and some selected nearby stations of GHBSN. The stations of GHBSN showed an overall higher background noise level for horizontal components than those of KMA in the long-period range. For the borehole broadband stations (stations JEJB and YOCB of the KMA network), the energy appears to decrease in the period below 0.8–0.9 s. This is mainly because the KMA borehole stations being compared have a hundred-meter deep-seated sensor, reducing surface noise, unlike sensors of GHBSN buried 1 m deep. Meanwhile, for the surface station (station DAG2 of the KMA network), both are comparable to each other in the high-frequency range suitable for microearthquake detection within the range of Peterson's noise model (Peterson, 1993) (Fig. 4).

## 4. EARTHQUAKE DETECTION AND ANALYSIS

### 4.1. Detecting and Locating Earthquakes

Earthquakes were detected from continuous seismic data using the following procedure. We used two programs, SeisComP and a program developed by Kim et al. (2018c), to detect earthquakes. They are independent of the crosschecks. Based on the outcomes of the two programs, we obtained the results of the earthquake coordinates after a manual review of the arrival times with a *Hypoellipse* for locating events (Lahr, 1999). The total number of events was 4,773. Artificial blast-like signals are observed during these events. Quarry blasts exhibit low-frequency pulses, as shown in Figure 3e (Korrat et al., 2022). If this event was located near a known quarry site within 3 km and during business hours (9–18), we classified it as a blast. If possible, the focal mechanism was determined based on the P-wave polarity (Snoke, 2003). We used a regional 1-D velocity model for the Gyeongsang Basin (Kim et al., 2011).

We here briefly summarize the processes in SeisComP and the program developed by Kim et al. (2018c). In SeisComP, the ratio of short-term to long-term averages (STA/LTA) is used to determine as many potential P waves as possible (Allen, 1978). From them, timings of P and S waves are measured via the method based on the Akaike information criterion (Maeda, 1985). The arrival times of common earthquakes were grouped (association) using the density-based spatial clustering of applications with noise (DBSCAN) method (Grigoli et al., 2018b). Earthquake coordinates were determined using the program *LocSAT* (Bratt and Bache, 1988).

In the program of Kim et al. (2018c), STA/LTA was used to determine potential P-waves. The program uses normalized squared envelope functions to measure the timings (Baer and Kradolfer, 1987). Outliers are filtered out under the assumption that P arrivals and the differences between S and P arrivals are linear (Wadati and Oki, 1933). The earthquake coordinates were determined using the program *Hypoellipse* (Lahr, 1999).

### 4.2. Local Magnitude

We developed a local magnitude scale for the southeastern region of South Korea using the earthquakes detected by the GHBSN. Given the observation range of the GHBSN and the magnitude range of the observed earthquakes, we considered that the KMA magnitude scale, which is based on a relatively broad observation range and earthquakes with a magnitude equal to or larger than 2.0 (Sheen et al., 2018), would make it challenging to accurately assess the magnitude of earthquakes observed by the GHBSN.

According to Richter (1935), the local magnitude scale ( $M_L$ ) is expressed as follows:

$$M_L = \log_{10} A - \log_{10} A_0 + S, \quad (1)$$

where  $A$  is the peak amplitude measured using the Wood-Anderson seismograph,  $\log_{10} A_0$  is the associated distance correction term, and  $S$  is the site correction term. Hutton and Boore (1987) proposed a modified distance correction term, written as follows:

$$-\log_{10} A_0 = n \log_{10} (R/17) + k (R - 17) + 2.0, \quad (2)$$

where  $n$  and  $k$  are parameters for the geometrical spreading and anelastic attenuation effects, respectively, and  $R$  is the hypocentral distance in km. The term  $\log_{10} A_0$  indicates that when a maximum amplitude of 10 mm is measured at a hypocentral distance of 17 km, the local magnitude is 3.

We used 2,860 earthquakes that were detected by at least 10 seismic stations to ensure high accuracy of the hypocenter and those that were located more than 3 km away from the quarry sites. This protocol was followed to ensure that the event was not an artificial blast. Excluding a 3 km area could rule out the unintended contribution of artificial earthquakes when establishing the local magnitude scale.

We preprocessed all the waveforms from the selected earthquakes as follows: removing the mean and linear trend, applying a bandpass filter at 2–20 Hz, removing the instrumental response, and convolving with the modified Wood-Anderson instrument response (Uhrhammer and Collins, 1990). The peak amplitude of the vertical component of each waveform was then measured. We determined the distance correction term using Equations (1)

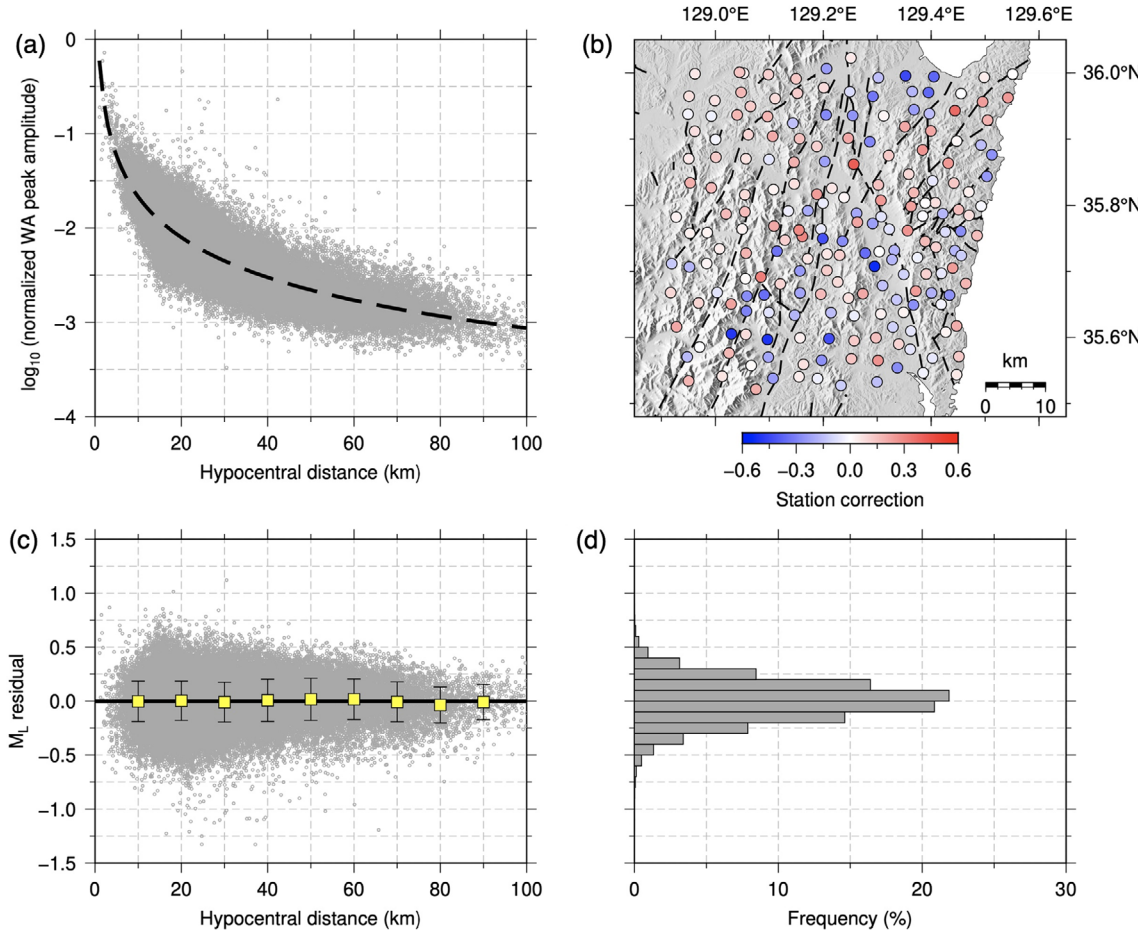


**Fig. 5.** (a) Logarithmic decay of the normalized Wood-Anderson (WA) amplitudes as a function of the hypocentral distance. The amplitudes were normalized with event magnitude and station corrections. The black dashed line denotes the attenuation correction curve. (b) Spatial distribution of the station correction terms obtained by inversion. The colors of the circles represent the correction scale for each station. (c) Magnitude residuals as a function of the hypocentral distance. The black solid line denotes linear regressions of the residuals. Each yellow square represents a mean of the residuals per 10 km intervals with the error bar for the standard deviation. (d) Histogram of the residuals.

and (2) and the peak amplitude through a generalized linear inversion. The developed distance correction term is expressed as follows:

$$-\log_{10} A_0 = 1.450676 \log_{10} (R/17) - 0.000661 (R - 17) + 2.0. \quad (3)$$

Figure 5 shows how the local magnitude scale was developed. The distance attenuation and logarithm of the normalized Wood-Anderson amplitudes as a function of hypocentral distance were well aligned (Fig. 5a). Station correction terms are associated with the individual site conditions and instrument installations for each seismic station (Miao and Langston, 2007; Kavoura et al., 2020). The station corrections of the GHBSN represent local site conditions because the stations of the GHBSN share the same installation conditions. Seismic stations with negative correction were predominantly observed in the valley region and their distribution corresponded to those with a high background noise level (Fig. 5b). This was likely related to the distribution of sedimentary rocks. The amplitudes at seismic

stations with high background noise levels were amplified. The  $M_L$  residuals were calculated as the difference between the station magnitudes obtained from a single station and the event magnitudes as the average station magnitudes for a given earthquake (Fig. 5c). The mean residuals at most of the distance ranges closely approached zero. This indicates that the distance and station corrections through the magnitude scale development adequately reflected the distance attenuation and site characteristics of the GHBSN-observed earthquakes.

#### 4.3. Statistics of Seismicity

The Gutenberg-Richter law represents the relationship between earthquake magnitude and frequency in any region and is generally expressed in the following form:

$$\log_{10} N(\geq M) = a - b M, \quad (4)$$

where  $N(\geq M)$  is the cumulative number of earthquakes with

magnitudes equal to or greater than  $M$  and  $a$  and  $b$  are constants that indicate the level of seismicity in any region. The b-value is related to the state of a material, the stress regime, and the distribution of fault segments in any region (Huang and Turcotte, 1988; Chan and Chandler, 2001; Schorlemmer et al., 2005). Generally, the global b-value is 0.7–1.0 in intraplate regions including the Korean Peninsula (Okal and Sweet, 2007).

The b-value for each dataset was calculated using the maximum likelihood method of Bender (1983) with a magnitude bin size

of 0.1. The standard error was estimated using the methods of Shi and Bolt (1982). We obtained a completeness magnitude ( $M_C$ ) above which all earthquakes are reliably recorded.  $M_C$  was estimated using the goodness-of-fit method suggested by Wiemer and Wyss (2000). We evaluated the  $M_C$  and b-value using the events detected after February 2019, which we think that the earthquake observation environment began to stabilize.

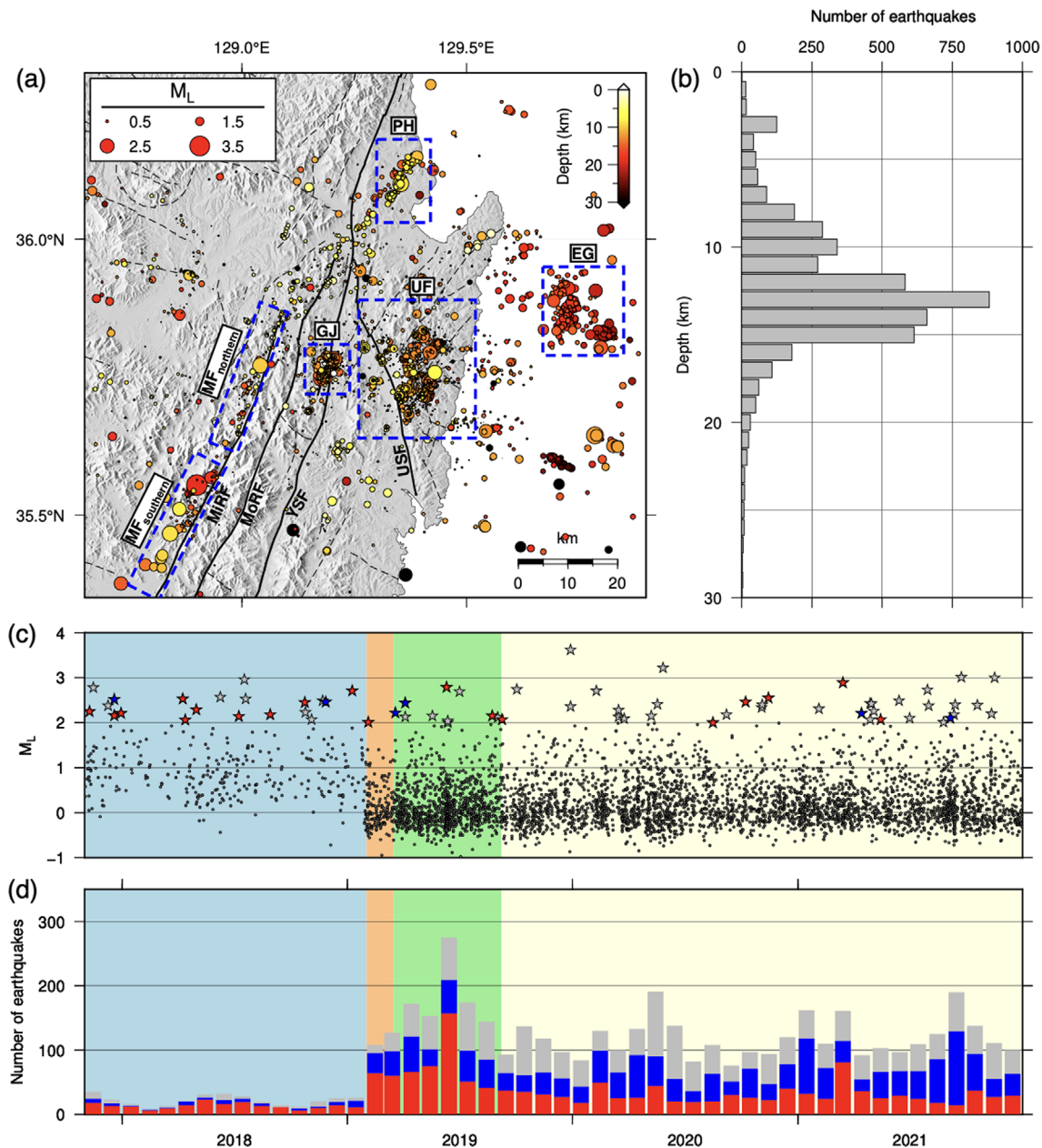


**Fig. 6.** Map of the seismicity probed with the GHBSN. (a) Map of the epicenters color-coded to depth. Blue dashed box indicates subregion classified to interest. (b) Histogram of focal depth. (c) Temporal distribution of earthquakes with magnitude. Red star is earthquake in GJ with magnitude larger than 2.0. Similarly, the blue star is for the UF. The others with magnitude greater than 2.0 are marked by gray star. (d) Histogram of temporal occurrence with bin of a month. Red and blue bars indicate the number of earthquakes in the GJ and the UF, respectively. The grey bar is for the other earthquakes. GJ: the 2016 Gyeongju earthquake region; UF: the eastern part of the Ulsan Fault; EG: the eastern offshore Gyeongju; MF: the western part of the Miryang Fault; PH: the 2017 Pohang earthquake region; USF: Ulsan Fault; MiRF: Miryang Fault.

## 5. SPATIOTEMPORAL EARTHQUAKE DISTRIBUTION

A total of 4,773 events that occurred in and around the GHBSN were detected from November 2017 to December 2021 (Fig. 6), with 3,935 of them occurring within the GHBSN ( $35.50^{\circ}\text{N}$ – $36.05^{\circ}\text{N}$ ,  $128.90^{\circ}\text{E}$ – $129.55^{\circ}\text{E}$ ). The event catalog for this study is shown in Table S1 (electronic supplementary material). The detected events can be categorized into several groups according to their distribution, that is, the 2016 Gyeongju earthquake region (GJ), eastern part of the Ulsan Fault (UF), 2017 Pohang earthquake region (PH), eastern offshore Gyeongju (EG), western part of the Miryang Fault (MF), and quarry blasting sites (Fig. 6). The numbers of earthquakes detected in the GJ, UF, PH, EG, and MF were 1,566, 1,587, 93, 131, and 292, respectively. The KMA reported 1,835 earthquakes in the area during the same period, and 223 (GJ), 150 (UF), 746 (PH), 49 (EG), and 38 (MF) earthquakes occurred in the clustered region. Excluding PH, the GHBSN demonstrated an outstanding performance in all regions. The difference in the number of earthquakes in the PH is because seven seismic stations of the GHBSN were adjacent to the GJ during the period when the aftershock activity of the 2017 Pohang earthquake was intense. We excluded earthquakes in the PH from the analysis because of the high uncertainty in determining the hypocenter and seismic source using the GHBSN.

During Phase I, 324 earthquakes were detected, with an average of approximately 21 earthquakes per 30 days (Fig. 6d). During phases II, III, and IV, approximately 108, 173, and 116 earthquakes were detected every 30 days, respectively (Fig. 6d). The number of observed earthquakes increased rapidly with the enlargement of the network, confirming the excellent performance of the

GHBSN. During phases II, III, and IV, a similar number of earthquakes was detected monthly, with higher frequencies occasionally reported. During Phase II, there was a substantial increase in the number of earthquakes. This was attributed to aftershock activity following the  $M_L$  2.8 earthquakes that occurred in the GJ on June 11, 2019. This phenomenon was occasionally observed when an earthquake with a magnitude of 2.0 or greater occurs in the GJ and UF. Except for the peaks, the number of earthquakes decreased smoothly from Phase II to Phase IV, including when the number of stations in GJ increased. The activity of aftershocks with magnitudes greater than or equal to 2.0 was not apparent in the KMA catalog. However, GHBSN detects microearthquakes that are not observable by regional seismic networks. Excluding this period, the number of earthquakes in GJ showed a slight decreasing trend over time.

### 5.1. The 2016 Gyeongju Earthquake Region (GJ)

A total of 1,566 earthquakes were detected in GJ by the GHBSN (Fig. 7). Earthquakes in GJ occur dominantly at depths ranging from 12 to 17 km. In the A1–A2 cross section (Fig. 7b), the dip of the fault plane imaged by the hypocenters was approximately  $70^{\circ}$ . The slope tended to become less steep at shallower depths. The area of seismicity in B1–B2 was  $6 \times 5 \text{ km}^2$ . The magnitude of the detected earthquakes ranged from –0.7 to 2.9, and these events were smaller than those previously reported (Son et al., 2018; Woo et al., 2019b). The fault-perpendicular view of B1–B2 shows the distribution of seismicity on the fault plane. Relatively low seismicity was observed at a depth of approximately 15 km.

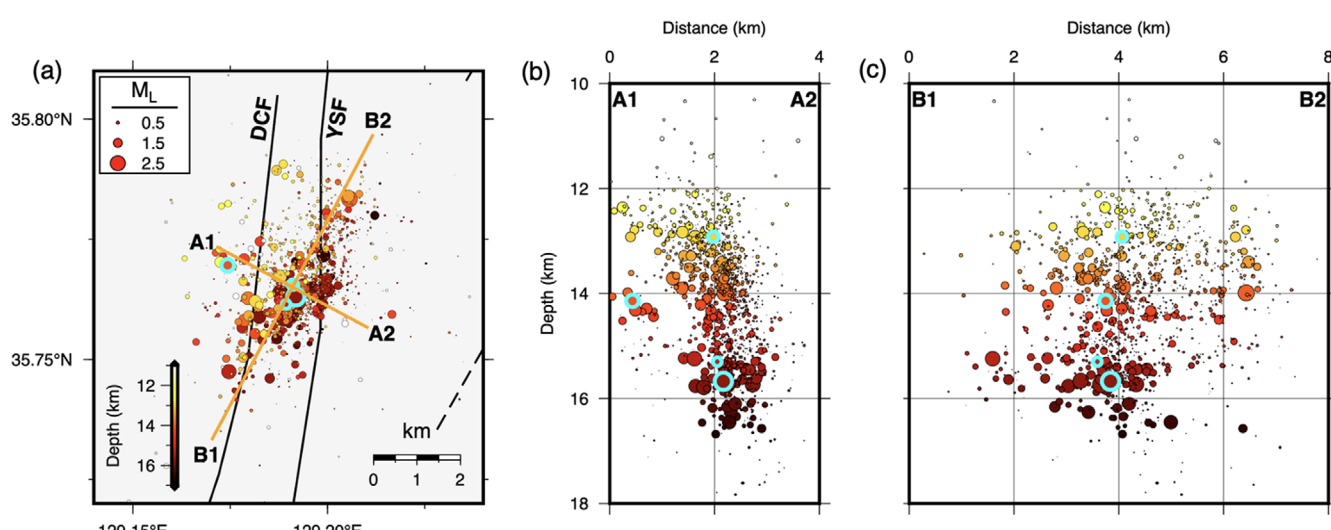


**Fig. 7.** Seismicity in the subregion GJ, including the aftershocks from the 2016  $M_W$  5.5 Gyeongju earthquake. (a) Map of the epicenters, color-coded to depth. (b) Cross-sectional view along A1–A2. (c) Cross-sectional view along B1–B2. Profiles A1–A2 and B1–B2 are indicated in orange lines in (a). Events in Figure 10 are marked with a thick sky-colored outline.

## 5.2. The Eastern Part of the Ulsan Fault (UF)

Based on our results, high seismic activity was observed in the UF. This region is known to undergo complex tectonic deformation (Kyung and Lee, 2006; Han et al., 2017). The spatial distribution of seismic activity in the UF is approximately  $15 \times 20 \text{ km}^2$ , which is broader than that in the GJ (Fig. 8). The focal depth was approximately 8–15 km. The magnitude of the detected earthquakes ranged from –0.6 to 2.5. Despite the infrequent occurrence of moderate-to-large earthquakes in the UF, microearthquake activity has continued to persist steadily during the operation period of the GHBSN. This is also evident in the estimated  $b$ -value, which was higher than those from other regions (Fig. 9). In cross sections A1–A2, the overall earthquake distribution showed an approximate dip of  $40^\circ$  (Fig. 8b). This is similar to the dip measured in the UF using surface geological surveys (Cheon et al., 2023). We also identified microearthquakes clustered along tectonic lines (Fig. 8). The complex hypocenter distribution is expected to be deeply connected to the geological deformation history in the UF.

## 5.3. The Eastern Offshore Gyeongju (EG), Western Part of the Miryang Fault (MF), and 2017 Pohang Earthquake Region (PH)

EG is known to have high seismicity (Kim et al., 2006b; Choi et al., 2012; Hong et al., 2020). The GHBSN was effective at detecting seismicity in this offshore region. The earthquakes in the EG occurred at a depth range of 15–25 km, which is deeper than that of land earthquakes. In the MF subregion, many earthquakes occurred linearly along the western part of the Miryang Fault. The MF developed with a trend similar to that of the Yangsan Fault. The distribution of earthquakes in the

western part of the MF has a long extension, and an  $M_L$  3.7 earthquake occurred on December 29, 2019. The hypocenter distribution in the MF exhibits distinct patterns in the northern and southern regions with the central part of the Miryang Fault. In the southern region, there is a relatively high frequency of large earthquakes. Only relatively large earthquakes at the epicenter of the 2017 Pohang earthquake were manually analyzed. The overall trend was similar to that of the NE-SW trending earthquake distribution shown by Lee et al. (2019) and Woo et al. (2020).

## 5.4. Completeness Magnitude ( $M_C$ ) and Gutenberg-Richter $b$ -value of the Microearthquake Catalog

We determined  $M_C$  values for all events and their subsets (Fig. 9). The  $M_C$  value for all events observed in this study was 0.0 (Fig. 9a). For the events that had epicenters inside the GHBSN, the  $M_C$  decreased slightly to –0.1. The  $M_C$  values were –0.2, 0.1, 0.7, 0.4, and –0.3 for the subregions GJ, UF, EG, southern MF, and northern MF, respectively (Fig. 9b–e). The heterogeneous level of ambient noise could affect the estimation of  $M_C$  at different locations (Fig. 4). The GHBSN improved  $M_C$  by approximately 3, in terms of  $M_C$  based on earthquakes from the regional seismic network operated by the KMA, 3.1 (Noh, 2019). Woo et al. (2019b) found events in the similar region of the GJ using the regional seismic and temporary networks. Their  $M_C$  was 1.0–1.3, which is larger than –0.2 of the GJ in this study. The  $M_C$  values could not be compared directly because Woo et al. (2019b) applied stricter filtering conditions in the double-difference relocation (Waldhauser and Ellsworth, 2000).

Similarly, the  $b$ -value in the Gutenberg-Richter relationship was calculated for various spatial zones. The  $b$ -values based on the whole events was  $0.84 \pm 0.02$  (Fig. 9a). It increased to  $1.01 \pm$

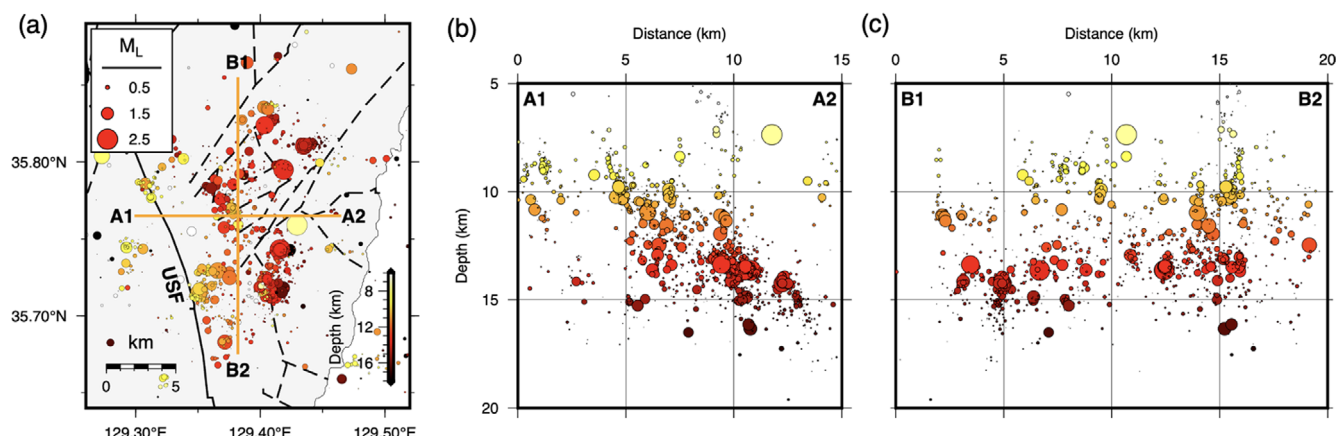


**Fig. 8.** Seismicity in the subregion UF, including seismicity between the USF and the coastline. (a) Map of the epicenters, color-coded to depth. (b) Cross-sectional view along A1–A2. (c) Cross-sectional view along B1–B2. Profiles A1–A2 and B1–B2 are indicated in orange lines in (a). USF: Ulsan Fault.

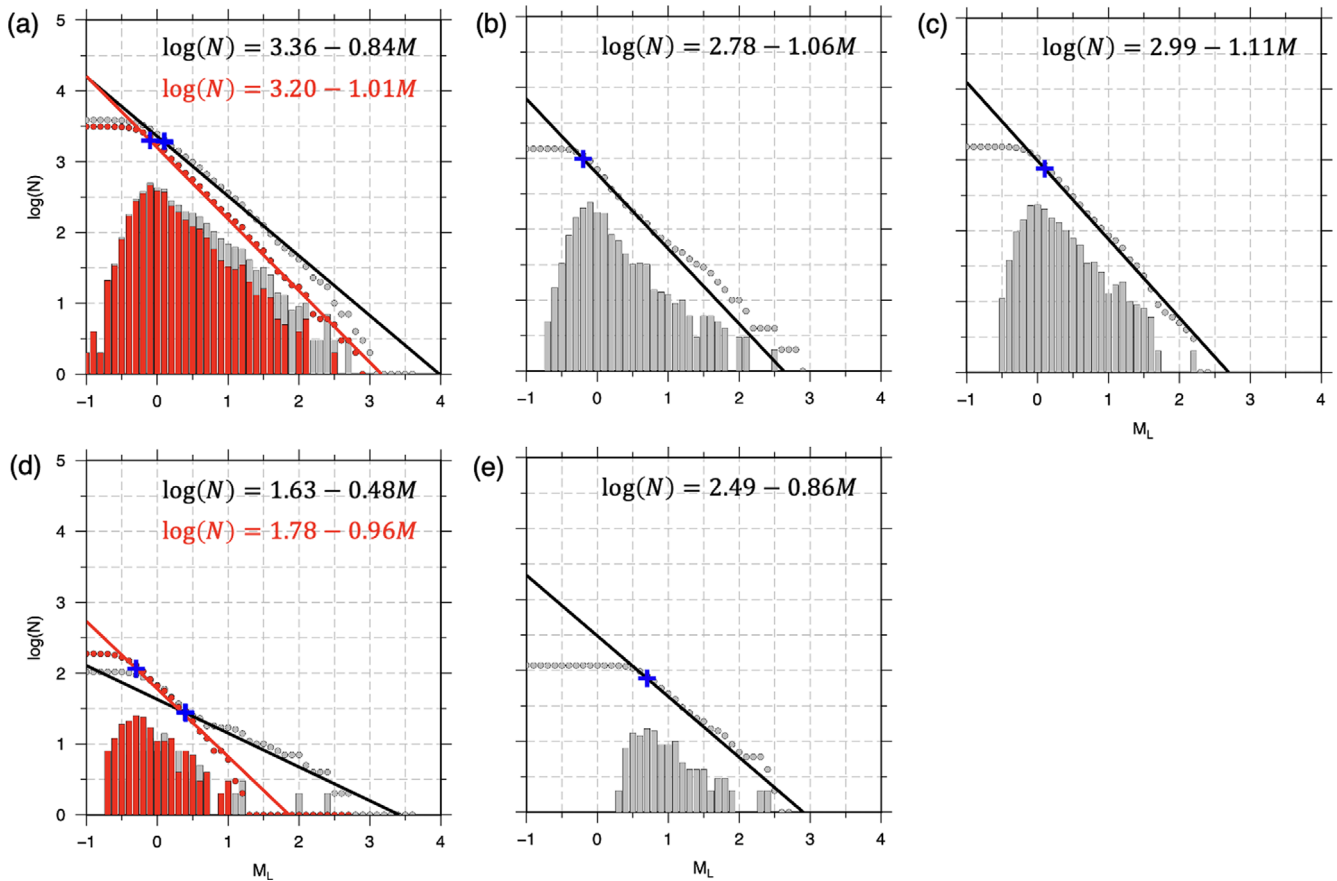


**Fig. 9.** Gutenberg-Richter (GR) relation about the cumulative number of earthquakes ( $N$ ) as a function of  $M_L$  in logarithmic scale, indicated by circles. The  $N$  at  $M_L = 1.2$  is defined as the number of earthquakes having  $M_L$  greater than or equal to 1.2. The absolute slope of the logarithmic  $N$ , fitted based on the maximum likelihood method, is the b-value. The differential  $N$  is plotted as histograms at the logarithmic scale. Blue crosses denote the  $M_C$ . (a) Catalog for the whole region in Figure 5a. Black lines, grey circles, and histograms are based on all the earthquakes. Red lines, circles, and histograms are based on the subset within the GHBSN. (b) GR relation for the subregion GJ. Similarly, (c), (d), and (e) are for the subregions UF, MF, and EG, respectively. The range of the subregion is shown in Figure 5. The catalog for the MF is divided into southern and northern parts plotted using black lines, grey circles, and histograms, and red lines, circles, and histograms, respectively.

0.02 when the events within the region of the GHBSN were counted (Fig. 9a). The b-values for the GJ, UF, EG, southern MF, and northern MF were  $1.06 \pm 0.03$ ,  $1.11 \pm 0.04$ ,  $0.86 \pm 0.09$ ,  $0.48 \pm 0.09$ , and  $0.96 \pm 0.08$ , respectively. Noh (2019) estimated the b-values as  $1.2 \pm 0.27$  using the onshore earthquakes in South Korea based on the KMA catalog. Woo et al. (2019b) yielded similar b-values as 0.82–1.14 for the sequence of the 2016 Gyeongju earthquakes to this study in the GJ. However, their estimation was based on aftershocks from a different time period, from immediately after the occurrence of the mainshock to the next 100 days.

### 5.5. Performance Enhancement in Determining the Focal Mechanism

We examined how the GHBSN improved the quality of focal mechanism solutions compared to the regional seismic network.

Four events were selected with  $M_L$  ranging from 1.46 to 2.89 in Phase IV, when all 200 stations were operating (Fig. 10). We used 49 KMA stations within 100 km from the center of the GHBSN to simulate the performance of the regional seismic network. For a fair comparison, this area was wider than that of the GHBSN by one order of magnitude. Based on this simulated regional seismic network (SRSN), we calculated the focal mechanism after obtaining the hypocenter (Fig. 10). For two events with  $M_L = 2.07$  and  $M_L = 2.89$ , GHBSN and SRSN yielded similar solutions for the nodal planes. The solutions of the nodal planes in the SRSN for the event with  $M_L = 2.07$  ( $M_L = 1.8$  from KMA) depended on two stations near the center of the hemisphere, with a relatively high deviation. For the event with  $M_L = 1.75$ , the solutions of the nodal planes were different for the GHBSN and SRSN. When  $M_L$  was reduced to 1.46, the focal mechanism could not be determined within a narrow range of the solution space.

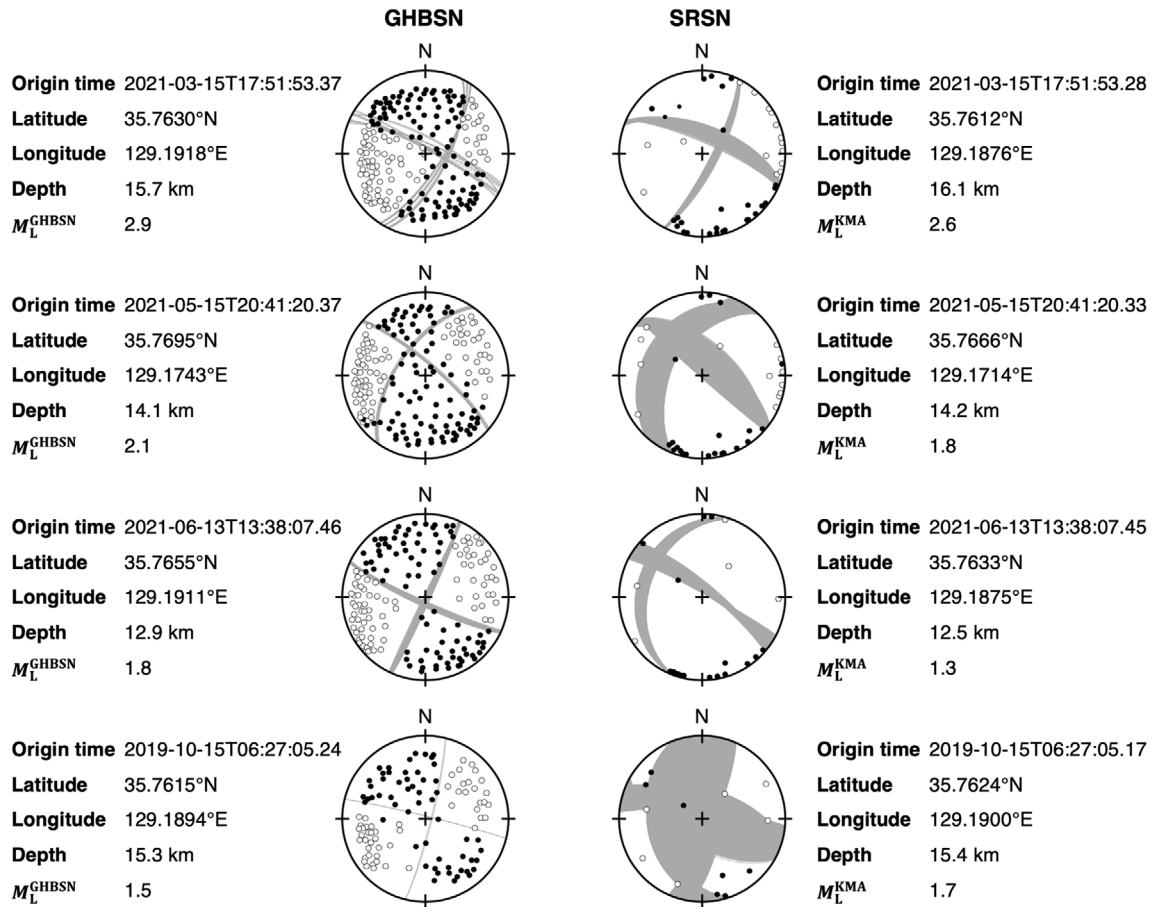


**Fig. 10.** Comparison of the determination of the focal mechanism when using the GHBSN and the simulated regional seismic network (SRSN) for four earthquakes in each row. The Left and right sides show results using the GHBSN and the SRSN, respectively.  $M_L^{\text{GHBSN}}$  stands for the magnitude estimated in this study, while the  $M_L^{\text{KMA}}$  is from the KMA earthquake catalog. Filled and open circles indicate compression and dilatation measured, respectively, in the lower hemisphere. Gray lines are the solution constrained by the measured polarities. N: North.

## 6. SUMMARY

Monitoring microearthquakes is essential for understanding the seismic characteristics of regions, particularly in intraplate settings. We constructed an extensive temporary seismic array, named GHBSN, to continuously monitor microseismicity in and around Gyeongju on the southeastern Korean Peninsula. The GHBSN was deployed in the area surrounding the epicenter of the 2016 Gyeongju earthquake between 2017 and 2019. The GHBSN comprised 200 seismic stations with an average inter-station distance of 4.5 km. A major purpose of the GHBSN is to investigate the subsurface causative fault with 3D geometry and slip responsible for the 2016 Gyeongju earthquake sequence, and the seismic characteristics and geological structures in the region. A significant increase in the number of earthquakes has been observed as the number of seismic stations has increased. Recorded high-density array data allowed for high-precision analysis of microearthquakes that occurred at the hypocenter of the 2016 Gyeongju earthquake.

We established a workflow to detect and analyze the continuous seismic data recorded by the GHBSN. Although the main target of the GHBSN was seismicity in the epicenter region of the 2016 Gyeongju earthquake, the detected events from the GHBSN were clustered in several other source areas in and around the network. These event-clustered areas were newly identified or confirmed from the GHBSN. This implies the contribution of the network to future seismic hazard evaluation of the region through the substantiation of seismic source identification. Most detected events were relatively small and were not observed in the regional seismic network. The GHBSN exhibited a significantly high performance in determining the hypocenter and focal mechanism solutions. As the magnitude decreased, the differences in the regional seismic network became more pronounced. Therefore, the GHBSN is expected to make significant progress in examining complex fault structures responsible for the 2016 Gyeongju earthquake sequence and in investigating the seismicity and geological structures of the southeastern Korean Peninsula.

## ACKNOWLEDGMENTS

This study was supported by the Nuclear Safety Research Program through the Korea Foundation of Nuclear Safety (KoFONS), using financial resources granted by the Nuclear Safety and Security Commission (NSSC) of the Republic of Korea (No. 1705010, 2203023). The authors thank Associate Editor Tae-Kyung Hong and the two reviewers for their valuable comments, which helped improve our manuscript.

## REFERENCES

- Ahern, T., Casey, R., Barnes, D., Benson, R., Knight, T., and Trabant, C., 2009, SEED reference manual, version 2.4. Incorporated Research Institutions for Seismology (IRIS), 220 p. [https://www.fdsn.org/pdf/SEEDManual\\_V2.4.pdf](https://www.fdsn.org/pdf/SEEDManual_V2.4.pdf) [Accessed on 6 February 2024].
- Allen, R.V., 1978, Automatic earthquake recognition and timing from single traces. *Bulletin of the Seismological Society of America*, 68, 1521–1532. <https://doi.org/10.1785/BSSA0680051521>
- Baer, M. and Kradolfer, U., 1987, An automatic phase picker for local and teleseismic events. *Bulletin of the Seismological Society of America*, 77, 1437–1445. <https://doi.org/10.1785/BSSA0770041437>
- Bender, B., 1983, Maximum likelihood estimation of *b* values for magnitude grouped data. *Bulletin of the Seismological Society of America*, 73, 831–851. <https://doi.org/10.1785/BSSA0730030831>
- Bratt, S.R. and Bache, T.C., 1988, Locating events with a sparse network of regional arrays. *Bulletin of the Seismological Society of America*, 78, 780–798. <https://doi.org/10.1785/BSSA0780020780>
- Chan, L. and Chandler, A., 2001, Spatial bias in *b*-value of the frequency-magnitude relation for the Hong Kong region. *Journal of Asian Earth Sciences*, 20, 73–81. [https://doi.org/10.1016/S1367-9120\(01\)00025-6](https://doi.org/10.1016/S1367-9120(01)00025-6)
- Chang, C., Lee, J.B., and Kang, T.-S., 2010, Interaction between regional stress state and faults: complementary analysis of borehole in situ stress and earthquake focal mechanism in southeastern Korea. *Tectonophysics*, 485, 164–177. <https://doi.org/10.1016/j.tecto.2009.12.012>
- Cheon, Y., Choi, J.-H., Choi, Y., Bae, H., Han, K.-H., Son, M., Choi, S.-J., and Ryoo, C.-R., 2020, Understanding the distribution and internal structure of the main core of the Yangsan Fault Zone: current trends and future work. *Journal of the Geological Society of Korea*, 56, 619–640. (in Korean with English abstract) <https://doi.org/10.14770/jgsk.2020.56.5.619>
- Cheon, Y., Sin, Y.H., Park, S., Choi, J.-H., Kim, D.-E., Ko, K., Ryoo, C.-R., Kim, Y.-S., and Son, M., 2023, Structural architecture and late Cenozoic tectonic evolution of the Ulsan Fault Zone, SE Korea: new insights from integration of geological and geophysical data. *Frontiers in Earth Science*, 11, 1183329. <https://doi.org/10.3389/feart.2023.1183329>
- Choi, H., Hong, T.-K., He, X., and Baag, C.-E., 2012, Seismic evidence for reverse activation of a paleo-rifting system in the East Sea (Sea of Japan). *Tectonophysics*, 572–573, 123–133. <https://doi.org/10.1016/j.tecto.2011.12.023>
- Chough, S.K., Kwon, S.-T., Ree, J.-H., and Choi, D.K., 2000, Tectonic and sedimentary evolution of the Korean peninsula: a review and new view. *Earth-Science Reviews*, 52, 175–235. [https://doi.org/10.1016/S0012-8252\(00\)00029-5](https://doi.org/10.1016/S0012-8252(00)00029-5)
- Chough, S.K. and Sohn, Y.K., 2010, Tectonic and sedimentary evolution of a Cretaceous continental arc-backarc system in the Korean peninsula: new view. *Earth-Science Reviews*, 101, 225–249. <https://doi.org/10.1016/j.earscirev.2010.05.004>
- Chwae, U.C., Kim, K.B., Hong, S.H., Lee, B.J., Hwang, J.H., Park, K.H., Hwang, S.K., Choi, P.Y., Song, K.Y., and Jin, M.S., 1995, Geological map of Korean (Scale 1:1,000,000). Korea Institute of Geology, Mining and Materials, Daejeon, South Korea.
- Grigoli, F., Cesca, S., Rinaldi, A.P., Manconi, A., López-Comino, J.A., Clinton, J.F., Westaway, R., Cauzzi, C., Dahm, T., and Wiemer, S., 2018a, The November 2017 Mw 5.5 Pohang earthquake: a possible case of induced seismicity in South Korea. *Science*, 360, 1003–1006. <https://doi.org/10.1126/science.aat2010>
- Grigoli, F., Scarabello, L., Böse, M., Weber, B., Wiemer, S., and Clinton, J.F., 2018b, Pick-and waveform-based techniques for real-time detection of induced seismicity. *Geophysical Journal International*, 213, 868–884. <https://doi.org/10.1093/gji/ggy019>
- Han, M., Kim, K.-H., Son, M., and Kang, S.Y., 2017, Current microseismicity and generating faults in the Gyeongju area, southeastern Korea. *Tectonophysics*, 694, 414–423. <https://doi.org/10.1016/j.tecto.2016.11.026>
- Helmholtz-Centre Potsdam – GFZ German Research Centre for Geosciences and GEMPA GmbH, 2008, The SeisComP seismological software package. GFZ Data Services. <https://doi.org/10.5880/GFZ.2.4.2020.003>
- Hong, T.-K., Lee, J., Kim, W., Hahm, I.-K., Woo, N.C., and Park, S., 2017, The 12 September 2016 M<sub>L</sub> 5.8 midcrustal earthquake in the Korean Peninsula and its seismic implications. *Geophysical Research Letters*, 44, 3131–3138. <https://doi.org/10.1002/2017GL072899>
- Hong, T.-K., Park, S., Lee, J., and Kim, W., 2020, Spatiotemporal seismicity evolution and seismic hazard potentials in the western East Sea (Sea of Japan). *Pure and Applied Geophysics*, 177, 3761–3774. <https://doi.org/10.1007/s00024-020-02479-z>
- Huang, J. and Turcotte, D.L., 1988, Fractal distributions of stress and strength and variations of *b*-value. *Earth and Planetary Science Letters*, 91, 223–230. [https://doi.org/10.1016/0012-821X\(88\)90164-1](https://doi.org/10.1016/0012-821X(88)90164-1)
- Hutton, L.K. and Boore, D.M., 1987, The M<sub>L</sub> scale in southern California. *Bulletin of the Seismological Society of America*, 77, 2074–2094. <https://doi.org/10.1785/BSSA0770062074>
- Hwang, B.-H., Lee, J.-D., and Yang, K., 2004, Petrological study of the granitic rocks around the Yangsan Fault: lateral displacement of the Yangsan Fault. *Journal of the Geological Society of Korea*, 40, 161–178. (in Korean with English abstract)
- Hwang, J.H., Jin, M.S., Jun, M.-S., Cho, J.D., Lee, S., Koo, S.B., Choi, P.-Y., Lee, Y.S., Kim, B.C., Kim, J.W., Kee, W.-S., Kang, P.C., Song, K.Y., Kim, J.H., Lee, S.R., and Chang, T.W., 2001, Tectonic Map of Korea (Scale 1:1,000,000). Korea Institute of Geoscience and Mineral Resources, Daejeon, South Korea.
- Jolivet, L., Tamaki, K., and Fournier, M., 1994, Japan Sea, opening history and mechanism: a synthesis. *Journal of Geophysical Research: Solid Earth*, 99, 22237–22259. <https://doi.org/10.1029/93JB03463>
- Jun, M.-S., 1990, Source parameters of shallow intraplate earthquakes in and around the Korean Peninsula and their tectonic implication. Ph.D. Thesis, Uppsala University, Uppsala, Sweden, 142 p.

- Jun, M.-S. and Jeon, J.-S., 2010, Focal mechanism in and around the Korean Peninsula. *Geophysics and Geophysical Exploration*, 13, 198–202. (in Korean with English abstract)
- Kang, T.-S. and Shin, J.S., 2006, Surface-wave tomography from ambient seismic noise of accelerograph networks in southern Korea. *Geophysical Research Letters*, 33, L17303. <https://doi.org/10.1029/2006GL027044>
- Kavoura F, Savvaidis, A., and Rathje, E., 2020, Determination of local magnitude for earthquakes recorded from the Texas Seismological Network (TexNet). *Seismological Society of America*, 91, 3223–3235. <https://doi.org/10.1785/0220190366>
- Kim, K.-H., Kang, T.-S., Rhie, J., Kim, Y., Park, Y., Kang, S.Y., Han, M., Kim, J., Park, J., Kim, M., Kong, C., Heo, D., Lee, H., Park, E., Park, H., Lee, S.-J., Cho, S., Woo, J.-U., Lee, S.-H., and Kim, J., 2016a, The 12 September 2016 Gyeongju earthquakes: 2. Temporary seismic network for monitoring aftershocks. *Geosciences Journal*, 20, 753–757. <https://doi.org/10.1007/s12303-016-0034-9>
- Kim, K.-H., Kim, J., Han, M., Kang, S.Y., Son, M., Kang, T.-S., Rhie, J., Kim, Y., Park, Y., Kim, H.-J., You, Q., and Hao, T., 2018a, Deep fault plane revealed by high-precision locations of early aftershocks following the 12 September 2016  $M_L$  5.8 Gyeongju, Korea, earthquake. *Bulletin of the Seismological Society of America*, 108, 517–523. <https://doi.org/10.1785/0120170104>
- Kim, K.-H., Ree, J.-H., Kim, Y., Kim, S., Kang, S.Y., and Seo, W., 2018b, Assessing whether the 2017  $M_W$  5.4 Pohang earthquake in South Korea was an induced event. *Science*, 360, 1007–1009. <https://doi.org/10.1126/science.aat6081>
- Kim, M., Kang, T.-S., Yoo, H.J., Rhie, J., Kim, Y., Kim, K.-H., and Park, Y., 2018c, Development of an automatic analysis algorithm for dense temporary seismic network and its application to the 2016  $M_L$  5.8 Gyeongju earthquake sequence, Korea. 2018 American Geophysical Union Fall Meeting, Washington, D.C., USA, Dec. 10–14, Abstract #S33E-0643.
- Kim, S., Rhie, J., and Kim, G., 2011, Forward waveform modelling procedure for 1-D crustal velocity structure and its application to the southern Korean Peninsula. *Geophysical Journal International*, 185, 453–468. <https://doi.org/10.1111/j.1365-246X.2011.04949.x>
- Kim, S.-K., Jun, M.-S., and Jeon, J.-S., 2006a, Recent research for the seismic activities and crustal velocity structure. *Economic and Environmental Geology*, 39, 369–384. (in Korean with English abstract)
- Kim, W.-Y., Noh, M.-H., and Choi, H.-S., 2006b, The 29 May 2004 offshore southeast coast of Korea earthquake sequence: shallow earthquakes in the Ulleung back-arc basin, East Sea (Sea of Japan). *Journal of the Korean Geophysical Society*, 9, 249–262.
- Kim, Y., He, X., Ni, S., Lim, H., and Park, S.-C., 2017, Earthquake source mechanism and rupture directivity of the 12 September 2016  $M_w$  5.5 Gyeongju, South Korea, earthquake. *Bulletin of the Seismological Society of America*, 107, 2525–2531. <https://doi.org/10.1785/0120170004>
- Kim, Y., Rhie, J., Kang, T.-S., Kim, K.-H., Kim, M., and Lee, S.-J., 2016b, The 12 September 2016 Gyeongju earthquakes: 1. Observation and remaining questions. *Geosciences Journal*, 20, 747–752. <https://doi.org/10.1007/s12303-016-0033-x>
- Korea Meteorological Administration, 2021, 2020 annual quality analysis report of seismic data. Korea Meteorological Administration, Seoul, South Korea, 514 p. (in Korean)
- Korrat, I.M., Lethy, A., ElGabry, M.N., Hussein, H.M., and Othman, A.S., 2022, Discrimination between small earthquakes and quarry blasts in Egypt using spectral source characteristics. *Pure and Applied Geophysics*, 179, 599–618. <https://doi.org/10.1007/s00024-022-02953-w>
- Kyung, J.B., 2003, Paleoseismology of the Yangsan fault, southeastern part of the Korean Peninsula. *Annals of Geophysics*, 46, 983–996. <https://doi.org/10.4401/ag-3465>
- Kyung, J.B. and Chang, T.W., 2001, The latest fault movement on the northern Yangsan fault zone around the Yugye-ri area, southeast Korea. *Journal of the Geological Society of Korea*, 37, 563–577. (in Korean with English abstract)
- Kyung, J.B. and Lee, K., 2006, Active fault study of the Yangsan fault system and Ulsan fault system, southeastern part of the Korean Peninsula. *Journal of the Korean Geophysical Society*, 9, 219–230.
- Lahr, J.C., 1999, revised 2012, HYPOELLIPE: a computer program for determining local earthquake hypocentral parameters, magnitude, and first motion pattern. USGS Open-File Report 99-23, version 1.1, U.S. Geological Survey, Reston, USA, 119 p.
- Lee, K. and Jin, Y.G., 1991, Segmentation of the Yangsan fault system: geophysical studies on major faults in the Kyeongsang basin. *Journal of the Geological Society of Korea*, 27, 434–449.
- Lee, K. and Yang, W.-S., 2006, Historical seismicity of Korea. *Bulletin of the Seismological Society of America*, 96, 846–855. <https://doi.org/10.1785/0120050050>
- Lee, K.-K., Ellsworth, W.L., Giardini, D., Townend, J., Ge, S., Shimamoto, T., Yeo, I.-W., Kang, T.-S., Rhie, J., Sheen, D.-H., Chang, C., Woo, J.-U., and Langenbruch, C., 2019, Managing injection-induced seismic risks. *Science*, 364, 730–732. <https://doi.org/10.1126/science.aax1878>
- Lim, H., Deng, K., Kim, Y.H., Ree, J.-H., Song, T.-R.A., and Kim, K.-H., 2020, The 2017  $M_w$  5.5 Pohang earthquake, South Korea, and poroelastic stress changes associated with fluid injection. *Journal of Geophysical Research: Solid Earth*, 125, e2019JB019134. <https://doi.org/10.1029/2019JB019134>
- Lim, H., Kim, Y., Kwon, K.B., Han, J., Ahn, B.S., Chai, G., Choi, Y., Heo, D., Jung, Y., Kang, H., Koh, M.H., Kwon, J., Park, J.Y., Seo, M.-S., Son, Y.O., Han, S., Kang, T.-S., Rhie, J., Kim, K.-H., and Ree, J.-H., 2021, Deployment of the linear array with geophones on the fault zone of the 2016  $M_w$  5.5 Gyeongju earthquake. *Journal of the Geological Society of Korea*, 57, 741–746. <http://doi.org/10.14770/jgsk.2021.57.5.741>
- Maeda, N., 1985, A method for reading and checking phase times in autoprocessing system of seismic wave data. *Zisin*, 38, 365–379. (in Japanese with English abstract) [https://doi.org/10.4294/zisin1948.38.3\\_365](https://doi.org/10.4294/zisin1948.38.3_365)
- McNamara, D.E. and Buland, R.P., 2004, Ambient noise levels in the continental United States. *Bulletin of the Seismological Society of America*, 94, 1517–1527. <https://doi.org/10.1785/012003001>
- Miao, Q. and Langston, C.A., 2007, Empirical distance attenuation and the local-magnitude scale for the central United States. *Bulletin of the Seismological Society of America*, 97, 2137–2151. <https://doi.org/10.1785/0120060188>
- Molnar, P. and Tapponnier, P., 1975, Cenozoic tectonics of Asia: effects of a continental collision. *Science*, 189, 419–426.

- Noh, M., 2019, Assessment of the completeness of earthquake catalogs. *Geosciences Journal*, 23, 253–263. <https://doi.org/10.1007/s12303-018-0028-x>
- Okal, E.A. and Sweet, J.R., 2007, Frequency-size distributions for intraplate earthquakes. In: Stein, S. and Mazzotti, S. (eds.), *Continental Intraplate Earthquakes: Science, Hazard, and Policy Issues*. Geological Society of America, Special Papers, 425, p. 59–71. [https://doi.org/10.1130/2007.2425\(05\)](https://doi.org/10.1130/2007.2425(05))
- Park, Y., Ree, J.-H., and Yoo, S.-H., 2006, Fault slip analysis of Quaternary faults in southeastern Korea. *Gondwana Research*, 9, 118–125. <https://doi.org/10.1016/j.gr.2005.06.007>
- Peterson, J., 1993, Observations and modeling of seismic background noise. USGS Open-File Report 93-322, U.S. Geological Survey, Reston, USA, 95 p. <https://doi.org/10.3133/ofr93322>
- Ree, J.-H., Lee, Y.-J., Rhodes, E.J., Park, Y., Kwon, S.-T., Chwae, U., Jeon, J.-S., and Lee, B., 2003, Quaternary reactivation of Tertiary faults in the southeastern Korean Peninsula: age constraint by optically stimulated luminescence dating. *Island Arc*, 12, 1–12. <https://doi.org/10.1046/j.1440-1738.2003.00372.x>
- Richter, C.F., 1935, An instrumental earthquake magnitude scale. *Bulletin of the Seismological Society of America*, 25, 1–32. <https://doi.org/10.1785/BSSA0250010001>
- Schorlemmer, D., Wiemer, S., and Wyss, M., 2005, Variations in earthquake-size distribution across different stress regimes. *Nature*, 437, 539–542. <https://doi.org/10.1038/nature04094>
- Seo, M.-S., Son, Y.O., Kim, Y., Kang, T.-S., Rhie, J., Kim, K.-H., and Ree, J.-H., 2022, Measurement of seismometer misorientation based on P-wave polarization: application to dense temporary broadband seismic array in the epicentral region of 2016 Gyeongju earthquake, South Korea. *Geosciences Journal*, 26, 385–397. <https://doi.org/10.1007/s12303-021-0041-3>
- Sheen, D.-H., Kang, T.-S., and Rhie, J., 2018, A local magnitude scale for South Korea. *Bulletin of the Seismological Society of America*, 108, 2748–2755. <https://doi.org/10.1785/0120180112>
- Shi, Y. and Bolt, B.A., 1982, The standard error of the magnitude-frequency b value. *Bulletin of the Seismological Society of America*, 72, 1677–1687. <https://doi.org/10.1785/BSSA0720051677>
- Snoke, J.A., 2003, FOCMEC: focal mechanism determinations. In: Lee, W.H.K., Kanamori, H., Jennings, P.C., and Kisslinger, C. (eds.), *International Handbook of Earthquake and Engineering Seismology*. International Geophysics Book Series, Academic Press, 81, p. 1629–1630. [https://doi.org/10.1016/S0074-6142\(03\)80291-7](https://doi.org/10.1016/S0074-6142(03)80291-7)
- Son, M., Cho, C.S., Shin, J.S., Rhee, H.-M., and Sheen, D.-H., 2018, Spatiotemporal distribution of events during the first three months of the 2016 Gyeongju, Korea, earthquake sequence. *Bulletin of the Seismological Society of America*, 108, 210–217. <https://doi.org/10.1785/0120170107>
- Talwani, P., 2017, On the nature of intraplate earthquakes. *Journal of Seismology*, 21, 47–68. <https://doi.org/10.1007/s10950-016-9582-8>
- Uchide, T. and Song, S.G., 2018, Fault rupture model of the 2016 Gyeongju, South Korea, earthquake and its implication for the underground fault system. *Geophysical Research Letters*, 45, 2257–2264. <https://doi.org/10.1002/2017GL076960>
- Uhrhammer, R.A. and Collins, E.R., 1990, Synthesis of Wood-Ander son seismograms from broadband digital records. *Bulletin of the Seismological Society of America*, 80, 702–716. <https://doi.org/10.1785/BSSA0800030702>
- Wadati, K. and Oki, S., 1933, On the travel time of earthquake waves (Part II). *Journal of the Meteorological Society of Japan, Series II*, 11, 14–28. (in Japanese with English abstract) [https://doi.org/10.2151/jmsj1923.11.1\\_14](https://doi.org/10.2151/jmsj1923.11.1_14)
- Waldhauser, F. and Ellsworth, W.L., 2000, A double-difference earthquake location algorithm: method and application to the northern Hayward Fault, California. *Bulletin of the Seismological Society of America*, 90, 1353–1368. <https://doi.org/10.1785/0120000006>
- Wiemer, S. and Wyss, M., 2000, Minimum magnitude of completeness in earthquake catalogs: examples from Alaska, the western United States, and Japan. *Bulletin of the Seismological Society of America*, 90, 859–869. <https://doi.org/10.1785/0119990114>
- Woo, J.-U., Kim, M., Rhie, J., and Kang, T.-S., 2020, Aftershock sequence and statistics of the 2017 M<sub>w</sub> 5.5 Pohang, South Korea, earthquake: implications of fault heterogeneity and postseismic relaxation. *Bulletin of the Seismological Society of America*, 110, 2031–2046. <https://doi.org/10.1785/0120200059>
- Woo, J.-U., Kim, M., Sheen, D.-H., Kang, T.-S., Rhie, J., Grigoli, F., Ellsworth, W.L., and Giardini, D., 2019a, An in-depth seismological analysis revealing a causal link between the 2017 M<sub>w</sub> 5.5 Pohang earthquake and EGS project. *Journal of Geophysical Research: Solid Earth*, 124, 13060–13078. <https://doi.org/10.1029/2019JB018368>
- Woo, J.-U., Rhie, J., Kim, S., Kang, T.-S., Kim, K.-H., and Kim, Y., 2019b, The 2016 Gyeongju earthquake sequence revisited: aftershock interactions within a complex fault system. *Geophysical Journal International*, 217, 58–74. <https://doi.org/10.1093/gji/ggz009>

**Publisher's Note** Springer Nature remains neutral with regard to jurisdictional claims in published maps and institutional affiliations.